ACS Photonics

Article

pubs.acs.org/journal/apchd5

Reducing the Complexity: Enantioselective Chiral Near-Fields by Diagonal Slit and Mirror Configuration

Martin Schäferling,*[,†] Nader Engheta,[‡] Harald Giessen,[†] and Thomas Weiss[†]

[†]4th Physics Institute, Research Center SCoPE, and Research Center SimTech, University of Stuttgart, Stuttgart, Germany

[‡]Department of Electrical and Systems Engineering, University of Pennsylvania, Philadelphia, Pennsylvania, United States

ABSTRACT: We report an easy-to-fabricate plasmonic design consisting of diagonal slits in a metallic film on top of a mirror for the generation of chiral near-fields of one single handedness. Our numerical investigations show that the distance between the two layers is crucial for the properties of this design. While the far-field response can be used to identify layer distances with strong chiral near-fields, this distance must be small enough to additionally ensure single-handedness of the respective fields close to the slit area. The fields of interest can be easily accessed by chiral molecules because they are located within the slits. Based on this finding, we propose and numerically verify a novel technique for chiroptical spectroscopy in a reflection geometry.

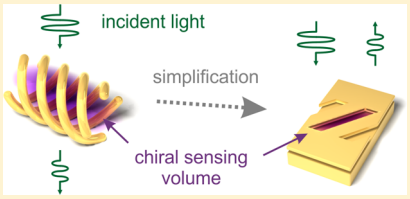

KEYWORDS: *optical chirality, plasmonics, near-field response, numerical simulation, simple nanostructure, chiroptical spectroscopy*

The term chirality is used to describe objects that cannot be superimposed with their mirror image.[1] This geometrical property is widely present in nature. A prominent example is the double-helical shape of DNA, but also most other biomolecules, such as the essential amino acids, are chiral.[2] Each of these molecules occurs in two enantiomeric forms, which are related by mirror symmetry. The handedness of a chiral molecule plays an important role in biochemical processes.[3] Reliable detection of the handedness with high sensitivity is therefore of major importance.

However, most physical properties that are commonly used to characterize a material are independent of its handedness; only interactions with other chiral objects result in a handedness-dependent response. A common technique for enantiomer discrimination is circular dichroism spectroscopy, which probes the difference in the absorption of left- and right-handed circularly polarized light.[4] However, this differential response is several orders of magnitude smaller than the achiral absorption of the incident light. Therefore, the analysis of small quantities or concentrations of a chiral analyte is challenging.

Plasmonic nanostructures—metallic geometries with feature sizes well below the wavelength of incident light—have been used to enhance small absorption signals of achiral molecules due to their capability to concentrate light in regions much smaller than the wavelength.[5] The plasmonic enhancement of a chiral response such as circular dichroism has been an active research topic for several years. It could be shown theoretically[6−9] and experimentally[10−17] that such an enhancement should, in principle, be possible.

Most theoretical investigations have focused on simple plasmonic nanustructures such as spheres, whose interaction with chiral molecules can be calculated analytically or semianalytically. The enhancement stems from interactions mediated by the electric field. A different approach can be found by analyzing the chiral properties of the electromagnetic field. They can be quantified via the so-called optical chirality C[18]

$$C = -\frac{\varepsilon_0 \omega}{2}\mathrm{Im}(\mathbf{E}^{*}\cdot\mathbf{B}) \tag{1}$$

which is a time-even pseudoscalar, that is, it changes its sign upon parity inversion similar to geometrically chiral objects. Here, $\mathbf{E}$ and $\mathbf{B}$ are the complex electric and magnetic fields, respectively, while ω is their angular frequency. Note that optical chirality is a measure for the helicity of monochromatic electromagnetic fields.[19−21]

It has been shown that the absorption of a chiral molecule in a monochromatic electromagnetic field can be written as[18,22]

$$A = \frac{2\omega}{\varepsilon_0}\mathrm{Im}(\alpha)U_\mathrm{e} + 2\mu_0\omega\mathrm{Im}(\chi)U_\mathrm{b} - \frac{2}{\varepsilon_0}\mathrm{Im}(\xi)C \tag{2}$$

Here, U_e and U_b denote the electric and magnetic energy density, respectively. The electric and magnetic dipole polarizability α and χ together with the so-called mixed electric-magnetic dipole polarizability ξ are material parameters. The latter is the only parameter that depends on the handedness of the chiral material; it changes its sign for the different enantiomers.[23] Therefore, the chiral interaction is described by the third term, where also the optical chirality of the electromagnetic field enters.

The differential absorption upon illumination with enantiomorphic fields, that is, $U^{+}_{\mathrm{e,b}} = U^{-}_{\mathrm{e,b}}$ and $C^{+} = -C^{-}$ can be written as

$$A^{+} - A^{-} \equiv \Delta A = -\frac{2}{\varepsilon_0}\mathrm{Im}(\xi)\Delta C \propto -\Delta C \equiv -(C^{+} - C^{-}) \tag{3}$$

Received: February 29, 2016
Published: May 9, 2016

DOI: 10.1021/acsphotonics.6b00147
ACS Photonics 2016, 3, 1076−1084

The superscripts denote the handedness of the respective fields. Positive optical chirality indicates left-handed fields. This definition is consistent with the detector's view convention for the handedness of circularly polarized light.

Equation 3 is an important result because it indicates that, in the weak coupling regime, the chiral interaction can be optimized by enhancing the optical chirality,[24] which is a property of the electromagnetic field. Maximum optical chirality in a plane wave is obtained for circularly polarized light:

$$C_{\mathrm{CPL}}^{\pm} = \pm\frac{\varepsilon_0\omega}{2c}|\mathbf{E}|^2 \tag{4}$$

Here, c is the speed of light.

It has been shown that plasmonic nanostructures can be used to create, enhance, and tailor chiral near-fields, thus, fields with nonzero optical chirality.[25,26] Geometrical chirality is not a necessary prerequisite for this purpose; rather, chiral near-fields also occur near achiral antennas[27−33] or even in completely achiral systems.[34,35] However, recent results indicate that geometrically chiral nanostructures do not only provide chiroptical far-field responses that are much stronger than for most natural molecules,[36] but are also favorable to optimize the chiroptical near-field response.[37]

In ref 37, we introduced a design consisting of multiple intertwined helices, which generates near-fields with an extended region where the optical chirality is more than 2 orders of magnitude stronger than that of circularly polarized light. Such a design maximizes optical chirality because of the parallel electric and magnetic field components inside the helices. A schematic of this design is shown in Figure 1 (top). However, the geometry of the design is complicated, which hampers fabrication. Nanohelices have been fabricated with various techniques, including direct laser writing,[38] glancing angle deposition,[39,40] electron- and focused ion-beam-induced deposition,[41−43] multiple-beam interference,[44] self-assembly techniques,[45,46] or a strain-induced roll-up method.[47] Recently, structures with three intertwined helices have been realized by a modified focused ion-beam induced deposition technique[48] and STED direct laser writing.[49] Nevertheless, these reports represent the top end of modern nanofabrication. Therefore, alternate designs, which are simpler to fabricate, are highly desirable.

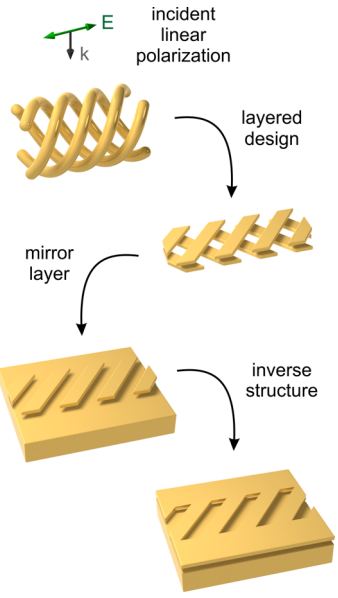

Figure 1. Steps to optimize a complex design of intertwined helices for practical applications. The structure is replaced by a two-layer design of diagonal stripes that mimics the current distribution of a helix. Then, the lower layer is replaced by a mirror to achieve better coupling between the layers. Finally, Babinet's principle is used to simplify the access of the chiral analyte to the areas with highest optical chirality.

Figure 1 visualizes the simplification process. We start with the initial design with four intertwined helices. The first reduction in complexity is obtained by replacing the helices with a two-layered design that consists of diagonal stripes. These stripes mimic the current distribution within the helix. However, coupling between these layers is a critical issue. It is nontrivial to optimize the structure because of the large amount of geometric parameters. Therefore, as a second step, the lower layer is replaced by a mirror. Hence, coupling between the layers only depends on their distance. Of course, this will not exactly mimic the current distribution obtained in the layered design. However, the induced mirror plasmons still result in a circular current distribution and, therefore, an effective magnetic dipole moment of the design. As a last step, the upper layer is replaced by its inverse structure. Babinet's principle ensures that the device still exhibits a chiroptical near-field response.[50] The usage of diagonal slits instead of stripes offers a natural way of adding the chiral analyte: It should be filled in the holes of the upper gold layer. The final diagonal-slit structure is simple to fabricate by standard electron-beam lithography because only a single nanostructured layer is present.

1. RESULTS AND DISCUSSION

To gain insights into the working principle of the diagonal-slit structure, we model it with a perfect electric conductor. The calculations have been performed with a commercial FEM solver (CST Microwave Studio, see Methods section for details). The design parameters are shown in Figure 2a. We used a width of 80 nm and a height of 250 nm for the slits. The upper right corner of the slit is sheared by 180 nm with respect to the lower right corner. Two neighboring slits are separated by 80 nm. The distance between two slit rows has been chosen as 300 nm. The thickness of the slit layer is 20 nm, the distance d_z to the mirror is tuned to optimize the response.

Figure 2b shows the obtained reflectance spectra for different layer distances d_z. The spectra have been calculated for incident vertically polarized light. Only the vertically polarized component of the reflected light is recorded. At resonance, the incident light is almost perfectly converted to the horizontally polarized state by the structure, which directly follows from the fact that neither transmittance nor absorbance can occur in the analyzed perfect electric conductor design. The same spectrum is obtained for incident horizontally polarized light. As a consequence of the perfect electric conductor, the resonance position has only a slight dependence on d_z, but the resonance width as well as the conversion efficiency are influenced.

The electric field vector must twist to perform the observed conversion of the polarization state. Therefore, we expect the near-fields to exhibit nonzero optical chirality; the handedness of the near-fields depends on the tilt direction of the slits. This expectation can be confirmed in Figure 3a. Here, we illuminated the structure for d_z = 20 nm, where the strongest resonance (and, therefore, the strongest polarization conversion) has been found. In this case, also the strongest chiral

DOI: 10.1021/acsphotonics.6b00147
ACS Photonics 2016, 3, 1076−1084

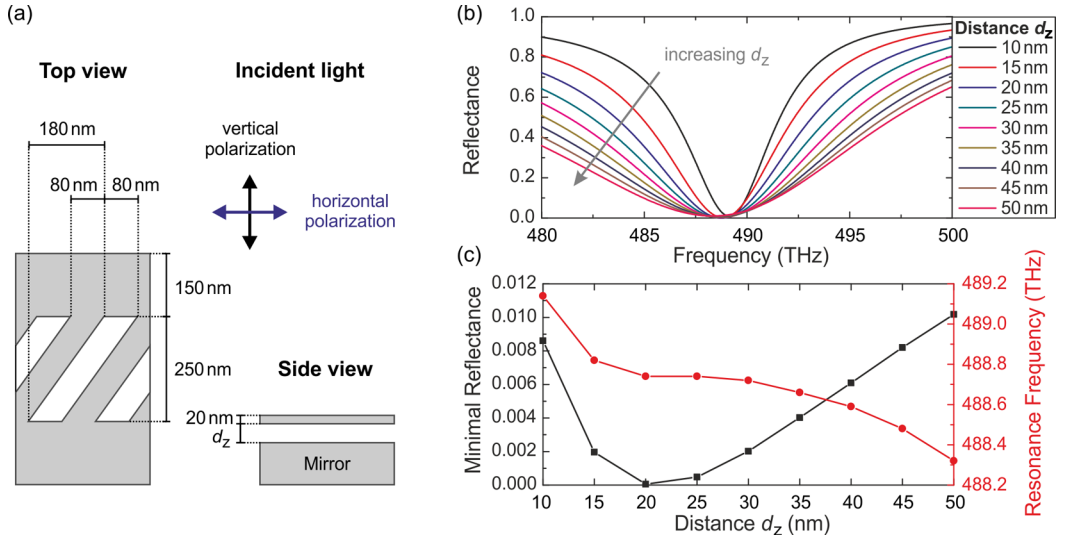

Figure 2. (a) Dimensions of the diagonal-slit structure that have been used for the calculations with a perfect electric conductor material. (b) Reflectance spectra for different layer distances d_z. (c) For a perfect electric conductor, only the minimal reflectance changes. The resonance frequency is only slightly altered.

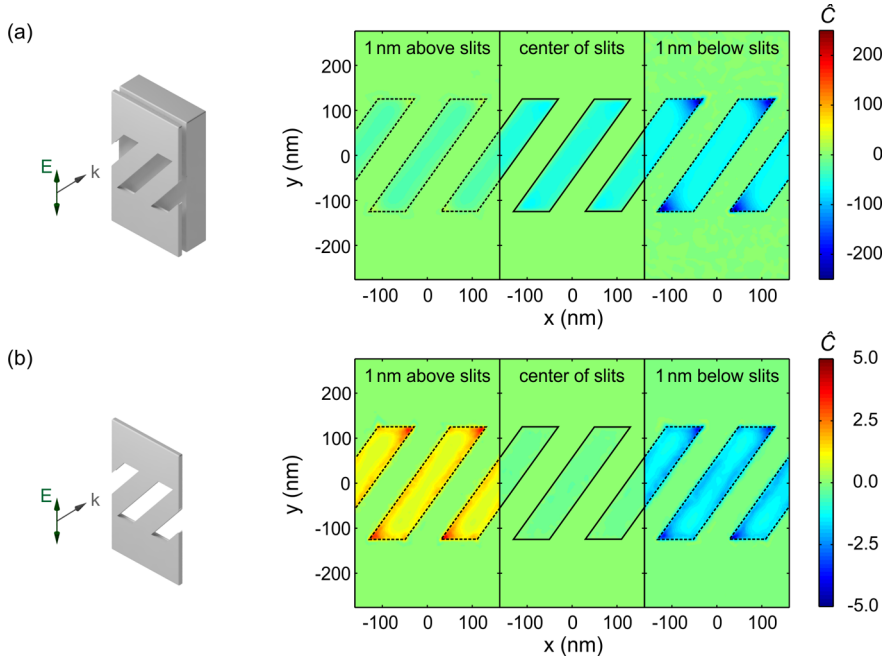

Figure 3. (a) Chiral near-fields obtained from the perfect electric conductor diagonal-slit structure with a layer distance d_z = 20 nm illuminated with vertically polarized light at resonance (488.7 THz, λ = 613.4 nm). Strong fields of one handedness are obtained in the whole slit. (b) Fields with opposite handedness above and below the slits are obtained when the mirror is removed. The resonance frequency changed to 483.8 THz (619.7 nm). The dashed lines indicate the positions of the slits in the close-by slit layer.

near-fields could be observed. Right-handed fields have been found above, below and in the center of the slit layer.

In Figure 3a, we plotted the optical chirality enhancement $\hat{C}$, which is obtained by normalizing the calculated optical chirality to the values of CPL (cf. eq 4):

$$\hat{C} \equiv \frac{C}{|C_{CPL}|} = -\frac{c\,\mathrm{Im}(\mathbf{E}^{*}\cdot\mathbf{B})}{|\mathbf{E}_{CPL}|^{2}} \tag{5}$$

Here, $\mathbf{E}_{CPL}$ is chosen such that the intensity and frequency of the corresponding circularly polarized plane wave matches those of the incident light. In doing so, the calculated values of $\hat{C}$ denote the enhancement compared to the maximum values obtained for comparable plane wave illumination. The sign of $\hat{C}$ still denotes the handedness of the chiral near-fields.

Figure 3b demonstrates that the behavior of the diagonal-slit structure depends crucially on the mirror. As soon as it is removed, the handednesses above and below the slits are opposite, while the optical chirality within the slit layer is almost vanishing. Additionally, the absolute values drop by a factor of more than 50 in the layer below the slit. This big difference is an additional indication of the strong influence of the mirror on the chiroptical near-field response of the system. As a benefit from the perfect electric conductor material, the resonance frequency shifts only slightly from 488.7 to

DOI: 10.1021/acsphotonics.6b00147
ACS Photonics 2016, 3, 1076−1084

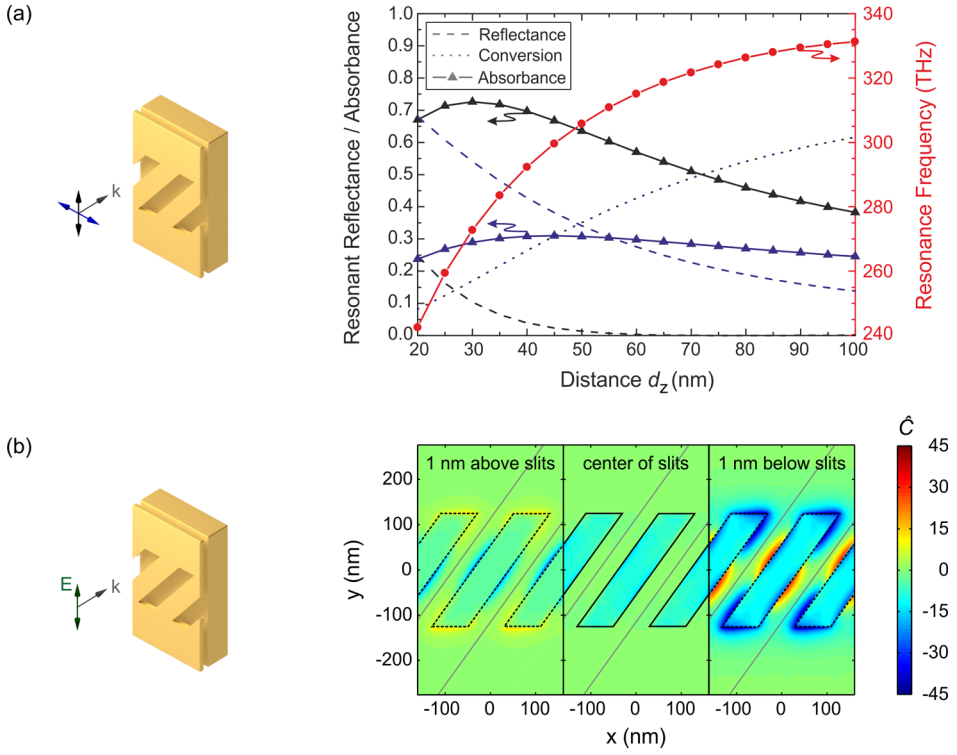

Figure 4. (a) Far-field response on resonance and corresponding resonance positions (red) for the diagonal-slit structure modeled with Drude gold. There is a strong difference in reflectance for vertically (black) and horizontally (blue) polarized incident light. The resonant absorbance (solid) is obtained from the reflectance (dashed) and the polarization conversion in reflection (dotted). For vertically polarized light, maximum absorbance is obtained at a layer distance of d_z = 30 nm (resonance frequency 272.8 THz, λ = 1098.9 nm). (b) At this distance, predominantly right-handed fields are observed within the slits. The black dashed lines indicate the positions of the slits in the close-by slit layer. The gray lines mark the borders of the inclined unit cell.

483.8 THz when the mirror is removed. Therefore, we can safely compare these two scenarios. For any realistic metal, a strong resonance shift would be expected, which might induce additional effects due to the dispersion of the metal.

This finding is consistent with earlier reports found in literature. Hendry and collaborators investigated an arrangement of two slits where the end of one slit is located near the center of the second slit to overlap the generated electric and magnetic near-fields.[51] They also found regions with left- and right-handed chiral near-fields on different sides of the structure. We expect this behavior to be linked to the symmetry of the structures. The slit layer alone is only chiral in two dimensions; in three dimensions, the enantiomorph can be obtained by simply flipping the structure around. This is impossible when the mirror, which breaks the symmetry in z-direction, is added: The diagonal-slit structure is geometrically chiral in three dimensions.

Although the absolute values of optical chirality are very strong for the analyzed diagonal-slit structure, they cannot be directly compared to other designs found in literature because of the perfect electric conductor. Therefore, we simulated the structure with the same geometry for a lossy metal. We used Drude parameters for gold in the near-infrared. The thickness of the mirror has been chosen as 100 nm, which is sufficient to suppress transmission. Different to the previous simulations, the calculations have been performed using an in-house code implenting the Fourier Modal Method with adaptive coordinates.[52] An inclined unit cell has been used for the calculations. Details about these simulations can be found in the Methods section.

The far-field behavior for different layer distances d_z is depicted in Figure 4a. In contrast to the perfect electric conductor, the reflectance (dashed) on resonance for vertically (blue) and horizontally (black) polarized incident light is clearly different. For these spectra, only the reflected polarization component that coincides with the incident polarization has been recorded. Additionally, a strong dependence of the resonance frequency on d_z is observed.

From a physical point of view, the important difference between a perfect electric conductor and gold is that, for gold, absorption can occur within the metal. Therefore, the layer distance with minimum reflectance will not necessarily lead to the strongest polarization conversion. In Figure 4a, polarization conversion in reflectance is depicted as dotted lines. Note that this response is the same for both incident polarizations.

Because the gold mirror has been chosen thick enough that the transmittance of the design is zero, one can directly calculate the absorbance (solid lines) by subtracting the sum of reflectance and polarization conversion from unity. We find maximum absorbance at a layer distance of 30 nm for vertically polarized light and at around 45 nm for horizontally polarized light.

In accordance with our findings in ref 37, we observed that the strongest chiral near-fields close to the slit could be observed at a layer distance that maximizes the absorption. The corresponding near-field response for incident vertically polarized light is depicted in Figure 4b. The values are significantly lower than for the perfect electric conductor, but we still obtain an enhancement of 1 order of magnitude compared to circularly polarized light of the same frequency in

DOI: 10.1021/acsphotonics.6b00147
ACS Photonics 2016, 3, 1076−1084

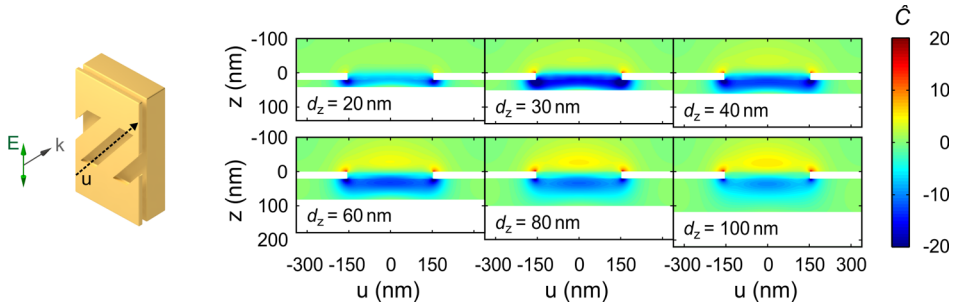

Figure 5. Chiral near-fields on a cut along the slit through the gold structure for different layer distances d_z (incident vertically polarized light). Between the slit and the mirror, the fields are right-handed. For increasing distance, the area with left-handed fields above the slit becomes more and more dominant. Strongest fields are observed for d_z = 30 nm, which corresponds to the distance with maximum absorbance (cf. Figure 4b).

the cut 1 nm below the slit layer. The chiral near-fields are right-handed within the whole slit area. Although we additionally find regions with left-handed chiral near-fields, those are located outside of this area. Therefore, they cannot be accessed by a chiral analyte that is present in the slits only.

For horizontally polarized light, the strongest response could be observed for d_z = 45 nm. However, this increase of the layer distance already leads to the occurrence of fields with opposite handedness closely above the slit layer. If we analyze the horizontal polarization at d_z = 30 nm, we find a similar distribution of chiral near-fields as for vertically polarized light (depicted in Figure 4b), but the absolute values are about three times smaller.

The occurrence of the opposite handedness for increasing layer distances can be explained by our calculations with the perfect electric conductor: If we remove the mirror, the chiral near-field response is highly symmetric, with fields of opposite handedness above and below the slits. Therefore, we can expect that such a behavior is approached when the mirror moves further apart and, accordingly, the coupling between slit layer and mirror becomes weaker. To further investigate this effect, we plotted the distribution of chiral near-fields along the propagation direction of the incident light. Figure 5 shows cuts through the structure along the slit for different layer distances d_z. We used vertically polarized incident light because it exhibits a stronger response than horizontal polarization. While the fields below the slits are right-handed, an area with left-handed fields is visible above the slit layer. With increasing layer distance, these fields gain in strength. Additionally, the right-handed fields within the slit become weaker. The plot confirms again that the strongest fields are obtained for d_z = 30 nm.

These findings result in two different aspects that have to be taken into account when optimizing the gold diagonal slit structure. First, the strength of the chiral near-field response is maximum for maximum absorbance. The absorbance shows a nontrivial dependence on d_z. The optimum layer distance depends on the incident polarization. The single-handedness of the fields, on the other hand, is best for small distances, which adds a constraint to the maximum distance that can be used. In our current design, a layer distance of d_z = 30 nm and incident vertically polarized light results in the best response. Therefore, these parameters are used in our subsequent analysis of potential chiroptical spectroscopy methods.

In the diagonal slit structure, the chiral near-fields are generated in a reflection geometry. Therefore, the chiroptical response of a chiral analyte placed in the slits will also be recorded in reflection. This is in contrast to common circular dichroism spectroscopy, which works in transmission. Classical circular dichroism spectroscopy cannot be applied in reflection because the incident circularly polarized light changes its handedness upon reflection. Therefore, no differential signal would be expected for the two incident circular polarizations.[53,54]

In Figure 6a, we sketched a potential scheme for chiroptical spectroscopy in reflection geometry based on our design. The

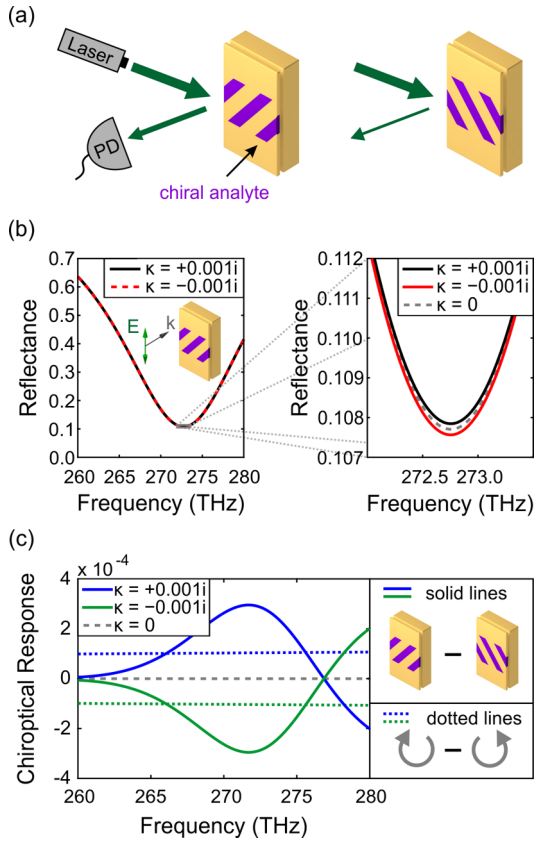

Figure 6. (a) Scheme of chiroptical spectroscopy in reflection geometry. The slits of two structures with opposite tilt are filled with a chiral analyte. The chiroptical response to detect is given by the differential reflectance. (b) The chiral analyte induces tiny changes into the reflectance spectrum depending on its handedness. The difference is only visible in the magnified plot close to the resonance. (c) The differential reflectance (solid lines) upon switching between the two structures can be used to detect the handedness of the chiral analyte. On resonance, the response is three times stronger than the circular dichroism signal of the same analyte (dotted lines). No chiroptical response is visible for the racemate (dashed gray line).

DOI: 10.1021/acsphotonics.6b00147
ACS Photonics 2016, 3, 1076−1084

chiral analyte is filled into the slits of two enantiomorphic diagonal-slit structures, i.e., with slits in opposite directions. This will generate enantiomorphic near-fields in the slit area. If each of these structures is measured independently, we expect a differential reflectance signal due to the different amount of energy that is absorbed by the chiral analyte. This signal depends on the handedness of the analyte and constitutes, therefore, a detectable chiroptical far-field response.

To substantiate this scheme, we perform additional numerical simulations of our design including the chiral analyte. The chiral constitutive equations[53,55]

$$\mathbf{D} = \varepsilon_0 \varepsilon \mathbf{E} - \frac{i\kappa}{c_0}\mathbf{H} \tag{6a}$$

$$\mathbf{B} = \mu_0 \mu \mathbf{H} + \frac{i\kappa}{c_0}\mathbf{E} \tag{6b}$$

have been used to account for the chiral medium. Here, $\mathbf{H}$ denotes magnetic field strength, while $\mathbf{D}$ is the electric displacement; c_0 is the speed of light in vacuum. The dimensionless material parameters entering this equation are the relative electric permittivity ε, the relative magnetic permeability μ, and, for chiral media, the so-called Pasteur parameter κ, which indicates the electric-magnetic cross-coupling. Different handedness of the chiral medium results in opposite sign of κ.

A homogeneous medium described with the constitutive equations (eqs 6) supports circularly polarized light as eigenpolarizations. The refractive index for the two orthogonal circular polarization states is given by

$$n_{\pm} = n \pm \kappa \tag{7}$$

A nonzero imaginary part of κ induces a difference in the absorption for left- and right-handed circularly polarized light.

For our analysis, we filled the slits with a chiral medium with $\varepsilon = 1 + 0.01i$ and $\mu = 1$ (resulting in $n = 1 + 0.005i$). The Pasteur parameter has to be chosen such that $\mathrm{Im}(n) > \mathrm{Im}(\kappa)$ to suppress artificial gain (cf. eq 7). We used $\kappa = 0 \pm 0.001i$ for our calculations.

Note that these parameters do not describe a realistic system. One would expect $\mathrm{Re}(\kappa) \gg \mathrm{Im}\,\kappa$ for realistic chiral materials far off the chiroptically active resonances, where the dispersion is approximately flat and constant values can be assumed. Depending on the system, one can find $\mathrm{Re}(\kappa) = 0$ around the resonances,[56,57] but κ is highly dispersive in these regions. However, we decided for now to consider such an artificial material to focus on the differential response of interest without distraction due to possible additional effects. The model should be adjusted for quantitative analysis of the proposed measurement scheme.

In such an analysis, one should additionally investigate the stability of the signal. One important source of noise, which is not present in conventional circular dichroism spectroscopy, arises due to the fact that two independent measurements on different enantiomorphs of the plasmonic structure have to be performed. Therefore, differences in local concentration of the chiral analyte might influence the observed signal. To minimize this effect, the number of slits (over which one averages during the measurment) should be chosen sufficiently large.

Figure 6b shows the calculated response for both enantiomers of our artificial chiral analyte. The parameters of the structure are the same as in Figure 4. The zoom-in shows a slight difference in reflectance depending on the handedness of the chiral analyte. As expected, this difference is symmetric around the response of the achiral racemic mixture (obtained by setting the Pasteur parameter $\kappa = 0$).

The response of our proposed measurement scheme, which detects the difference in reflectance for one chiral analyte filled into the two enantiomorphic diagonal-slit designs, is shown in Figure 6c. We obtain a nonzero differential response that peaks at the resonance frequency of the plasmonic nanostructure and is mirror-symmetric for the two enantiomers of the chiral analyte. The response for the racemic mixture vanishes within the numerical accuracy.

For comparison, we included the result when carrying out conventional circular dichroism spectroscopy (dotted lines) in the plot. For this, we calculated the differential transmittance of right- and left-handed circularly polarized light without the nanostructure. On resonance, our proposed scheme enhances the response by a factor of roughly 3. A stronger response might be obtained by further improving the geometry of the structure or by optimizing the region where the analyte is filled in. Nevertheless, these results demonstrate that, using plasmonic nanostructures, chiroptical spectroscopy with linearly polarized light in a reflection geometry is possible and can result in stronger responses than conventional circular dichroism spectroscopy.

The obtained enhancement factor is independent of κ because ΔA is directly proportional to ΔC. Therefore, measurement schemes incorporating enantiomorphic fields can be directly compared via analyzing ΔC without taking any specific chiral analyte into account. The absolute strength of the differential response, however, scales with κ. Therefore, the best performance of the proposed spectrocopy scheme is expected when the plasmon resonance is tuned to the chiroptically active resonance of the analyte. In this case, the ratio between the imaginary and the real part of the Pasteur parameter is highest as well, which minimizes additional influences of the real part.

Modern chiroptical spectroscopy probes both electronic transitions and vibrational resonances.[4,58] Electronic transitions are usually located in the ultraviolet wavelength region, where no plasmonic resonances can be observed for gold. There have been several different metals suggested for ultraviolet plasmonics,[59] but they are more complicated to handle. Vibrational resonances, on the other hand, can be found in the near- and mid-infrared regime, which is an excellent operation range for gold nanostructures. Therefore, we expect our proposed design to be well-suited for plasmonically enhanced vibrational circular dichroism spectroscopy.

2. CONCLUSION

We have shown how to simplify an optimized design for the generation of strong chiral near-fields. The resulting diagonal-slit structure with one nanostructured layer on top of a metallic mirror is straightforward to fabricate with conventional electron-beam lithography. Chiral near-fields of one handedness are generated within the slits. Therefore, they are easy to access for a chiral analyte, rendering this design as a promising candidate for plasmonically enhanced chiroptical spectroscopy.

The response of the structure strongly depends on the distance between the slit layer and the mirror. Depending on the material, different far-field responses can be used to identify layer distances with strong chiral near-fields. For a perfect electric conductor, the strongest response is observed at minimum reflectance, which results in maximum polarization

DOI: 10.1021/acsphotonics.6b00147
ACS Photonics 2016, 3, 1076−1084

conversion. For gold, on the other hand, the absorption of the structure should be maximized. Additionally, the layer distance should be chosen small enough that only one handedness of chiral near-fields occurs close to the slits. Although this might lower the absolute values of optical chirality, single-handedness of the fields is of major importance for any application based on these fields and should, therefore, be ensured.

Based on our design, we proposed a novel method for chiroptical spectroscopy that works in reflection. This might be interesting for applications such as remote sensing, where illumination and detection should happen within the same unit. First simulations of the whole device (including the chiral analyte) confirmed the viability of this scheme. We could even demonstrate an enhancement of the signal compared to conventional circular dichroism spectroscopy. More sophisticated models for the chiral analyte would be necessary to obtain a more precise prediction of the quantitative sensitivity of our proposed scheme when using real-life chiral liquids.

Note that we do not provide fully optimized geometries, but demonstrate the general working principle of our structure. Further geometrical optimization might lead to stronger chiral near-fields. However, further work is necessary to understand and optimize the in-plane coupling between the single slits. Additional modifications of the structure might lead to a geometry where the handedness of the chiral near-fields can be switched by the incident polarization instead of the tilt direction of the slits.

3. METHODS

3.1. FEM Calculations. The calculations shown in Figures 2 and 3 have been performed with the commercially available software package CST Studio Suite 2014. We used a second-order frequency domain solver and a tetrahedral grid. The dimensions of the simulations can be obtained from Figure 2a. The unit cell covers exactly the area depicted in the field plots (Figure 3). Its size is 320 nm × 550 nm. The structure has been embedded in air.

3.2. Fourier Modal Method Calculations. All calculations incorporating lossy metals (Figures 4 and 6) have been performed with an in-house implementation of the Fourier Modal Method with adaptive coordinates. The number of harmonics in the Fourier expansion has been chosen such that convergence has been reached. We adapted the Drude parameters from ref 60 for gold in the near-infrared: $\omega_p = 1.37 \times 10^{16}$ rad/s, $\gamma = 1.22 \times 10^{14}$ rad/s.

In our calculations, an inclined unit cell incorporating only one slit has been used (cf. solid gray lines in Figure 4). The size of the inclined unit cell is 160 nm × 550 nm/cos ζ with an inclination angle of $\zeta = -\tan^{-1}$ (180/250 nm). Comparison with the rectangular unit cell used in CST Microwave Studio lead to similar results. All other geometric parameters were the same as for the perfect electric conductor design.

For the implementation of the chiral analyte, our code has been extended to the chiral constitutive eqs 6. For that, we extended the formulation of Onishi et al.[61] to biperiodic gratings. Our implementation includes the correct factorization rules for chiral media in accordance to those of achiral media[62] to ensure optimum convergence. Only the holes in the slit layer have been filled with the chiral analyte. The spacer layer between the slit layer and the mirror is filled with air. The analysis of the racemate (with theoretically zero chiroptical response) gives an estimate for the error occurring in the calculations. We obtain chiroptical responses below 10^{-10}, which results in an error much lower than the accuracy needed for the presented results. The results for a numerical circular dichroism experiment have been obtained by removing the metal completely. Only the region of the former slit has been filled with the chiral analyte to ensure that the same amount of analyte has been used for the detection. In this configuration, differential transmittance of right- and left-handed circularly polarized light has been detected as chiroptical response.

AUTHOR INFORMATION

Corresponding Author

*E-mail: m.schaeferling@pi4.uni-stuttgart.de.

Notes

The authors declare no competing financial interest.

ACKNOWLEDGMENTS

The authors thank Uday K. Chettiar for helpful discussions. Parts of this work have been financially supported by Baden-Württemberg Stiftung, BMBF, DFG, and ERC (COMPLEXPLAS). N.E. acknowledges a MPI-FKF guest professorship at the 4th Physics Institute of the University of Stuttgart.

REFERENCES

(1) Kelvin, W. T. *Baltimore Lectures on Molecular Dynamics and the Wave Theory of Light*; CJ Clay and Sons: London, 1904.
(2) Meierhenrich, U. *Amino Acids and the Asymmetry of Life*; Springer: Berlin, 2008.
(3) Siegel, J. S. Biochemistry. Single-handed cooperation. *Nature* **2001**, *409*, 777−778.
(4) Berova, N., Nakanishi, K., Woody, R. W., Eds. *Circular Dichroism: Principles and Applications*, 2nd ed.; Wiley-VCH: New York, 2000.
(5) Neubrech, F.; Pucci, A.; Cornelius, T.; Karim, S.; García-Etxarri, A.; Aizpurua, J. Resonant Plasmonic and Vibrational Coupling in a Tailored Nanoantenna for Infrared Detection. *Phys. Rev. Lett.* **2008**, *101*, 157403.
(6) Govorov, A. O. Plasmon-Induced Circular Dichroism of a Chiral Molecule in the Vicinity of Metal Nanocrystals. Application to Various Geometries. *J. Phys. Chem. C* **2011**, *115*, 7914−7923.
(7) Zhang, H.; Govorov, A. O. Giant circular dichroism of a molecule in a region of strong plasmon resonances between two neighboring gold nanocrystals. *Phys. Rev. B: Condens. Matter Mater. Phys.* **2013**, *87*, 075410.
(8) Chulhai, D. V.; Jensen, L. Plasmonic Circular Dichroism of 310- and α-Helix Using a Discrete Interaction Model/Quantum Mechanics Method. *J. Phys. Chem. A* **2015**, *119*, 5218−5223.
(9) Nesterov, M. L.; Yin, X.; Schäferling, M.; Giessen, H.; Weiss, T. The Role of Plasmon-Generated Near Fields for Enhanced Circular Dichroism Spectroscopy. *ACS Photonics* **2016**, *3*, 578−583.
(10) Hendry, E.; Carpy, T.; Johnston, J.; Popland, M.; Mikhaylovskiy, R. V.; Lapthorn, A. J.; Kelly, S. M.; Barron, L. D.; Gadegaard, N.; Kadodwala, M. Ultrasensitive detection and characterization of biomolecules using superchiral fields. *Nat. Nanotechnol.* **2010**, *5*, 783−787.
(11) Govorov, A. O.; Gun'ko, Y. K.; Slocik, J. M.; Gérard, V. A.; Fan, Z.; Naik, R. R. Chiral nanoparticle assemblies: circular dichroism, plasmonic interactions, and exciton effects. *J. Mater. Chem.* **2011**, *21*, 16806−16818.
(12) Ben-Moshe, A.; Maoz, B. M.; Govorov, A. O.; Markovich, G. Chirality and chiroptical effects in inorganic nanocrystal systems with plasmon and exciton resonances. *Chem. Soc. Rev.* **2013**, *42*, 7028−7041.
(13) Lu, F.; Tian, Y.; Liu, M.; Su, D.; Zhang, H.; Govorov, A. O.; Gang, O. Discrete nanocubes as plasmonic reporters of molecular chirality. *Nano Lett.* **2013**, *13*, 3145−3151.

DOI: 10.1021/acsphotonics.6b00147
ACS Photonics 2016, 3, 1076−1084

(14) Ma, W.; Kuang, H.; Xu, L.; Ding, L.; Xu, C.; Wang, L.; Kotov, N. A. Attomolar DNA detection with chiral nanorod assemblies. *Nat. Commun.* **2013**, *4*, 2689.
(15) Wu, X.; Xu, L.; Liu, L.; Ma, W.; Yin, H.; Kuang, H.; Wang, L.; Xu, C.; Kotov, N. A. Unexpected chirality of nanoparticle dimers and ultrasensitive chiroplasmonic bioanalysis. *J. Am. Chem. Soc.* **2013**, *135*, 18629−18636.
(16) Wang, R.-Y.; Wang, P.; Liu, Y.; Zhao, W.; Zhai, D.; Hong, X.; Ji, Y.; Wu, X.; Wang, F.; Zhang, D.; Zhang, W.; Liu, R.; Zhang, X. Experimental Observation of Giant Chiroptical Amplification of Small Chiral Molecules by Gold Nanosphere Clusters. *J. Phys. Chem. C* **2014**, *118*, 9690−9695.
(17) Tullius, R.; Karimullah, A. S.; Rodier, M.; Fitzpatrick, B.; Gadegaard, N.; Barron, L. D.; Rotello, V. M.; Cooke, G.; Lapthorn, A.; Kadodwala, M. "Superchiral" Spectroscopy: Detection of Protein Higher Order Hierarchical Structure with Chiral Plasmonic Nanostructures. *J. Am. Chem. Soc.* **2015**, *137*, 8380−8383.
(18) Tang, Y.; Cohen, A. E. Optical Chirality and Its Interaction with Matter. *Phys. Rev. Lett.* **2010**, *104*, 163901.
(19) Bliokh, K.; Nori, F. Characterizing optical chirality. *Phys. Rev. A: At., Mol., Opt. Phys.* **2011**, *83*, 021803.
(20) Coles, M. M.; Andrews, D. L. Chirality and angular momentum in optical radiation. *Phys. Rev. A: At., Mol., Opt. Phys.* **2012**, *85*, 063810.
(21) Philbin, T. G. Lipkin's conservation law, Noether's theorem, and the relation to optical helicity. *Phys. Rev. A: At., Mol., Opt. Phys.* **2013**, *87*, 043843.
(22) Choi, J. S.; Cho, M. Limitations of a superchiral field. *Phys. Rev. A: At., Mol., Opt. Phys.* **2012**, *86*, 063834.
(23) Barron, L. D. *Molecular Light Scattering and Optical Activity*, 2nd ed.; Cambridge University Press: Cambridge, 2004.
(24) Tang, Y.; Cohen, A. E. Enhanced enantioselectivity in excitation of chiral molecules by superchiral light. *Science* **2011**, *332*, 333−336.
(25) Schäferling, M.; Dregely, D.; Hentschel, M.; Giessen, H. Tailoring Enhanced Optical Chirality: Design Principles for Chiral Plasmonic Nanostructures. *Phys. Rev. X* **2012**, *2*, 031010.
(26) Meinzer, N.; Hendry, E.; Barnes, W. L. Probing the chiral nature of electromagnetic fields surrounding plasmonic nanostructures. *Phys. Rev. B: Condens. Matter Mater. Phys.* **2013**, *88*, 041407.
(27) Biagioni, P.; Savoini, M.; Huang, J.-S.; Duò, L.; Finazzi, M.; Hecht, B. Near-field polarization shaping by a near-resonant plasmonic cross antenna. *Phys. Rev. B: Condens. Matter Mater. Phys.* **2009**, *80*, 153409.
(28) García-Etxarri, A.; Dionne, J. A. Surface-enhanced circular dichroism spectroscopy mediated by nonchiral nanoantennas. *Phys. Rev. B: Condens. Matter Mater. Phys.* **2013**, *87*, 235409.
(29) Yoo, S.; Cho, M.; Park, Q.-H. Globally enhanced chiral field generation by negative-index metamaterials. *Phys. Rev. B: Condens. Matter Mater. Phys.* **2014**, *89*, 161405.
(30) Lin, D.; Huang, J.-S. Slant-gap plasmonic nanoantennas for optical chirality engineering and circular dichroism enhancement. *Opt. Express* **2014**, *22*, 7434−7445.
(31) Liu, Y.; Zhao, W.; Ji, Y.; Wang, R.-Y.; Wu, X.; Zhang, X. D. Strong superchiral field in hot spots and its interaction with chiral molecules. *Europhys. Lett.* **2015**, *110*, 17008.
(32) Alizadeh, M. H.; Reinhard, B. M. Plasmonically Enhanced Chiral Optical Fields and Forces in Achiral Split Ring Resonators. *ACS Photonics* **2015**, *2*, 361−368.
(33) Tian, X.; Fang, Y.; Sun, M. Formation of Enhanced Uniform Chiral Fields in Symmetric Dimer Nanostructures. *Sci. Rep.* **2015**, *5*, 17534.
(34) Schäferling, M.; Yin, X.; Giessen, H. Formation of chiral fields in a symmetric environment. *Opt. Express* **2012**, *20*, 26326−26336.
(35) Davis, T. J.; Hendry, E. Superchiral electromagnetic fields created by surface plasmons in nonchiral metallic nanostructures. *Phys. Rev. B: Condens. Matter Mater. Phys.* **2013**, *87*, 085405.
(36) Valev, V. K.; Baumberg, J. J.; Sibilia, C.; Verbiest, T. Chirality and Chiroptical Effects in Plasmonic Nanostructures: Fundamentals, Recent Progress, and Outlook. *Adv. Mater.* **2013**, *25*, 2517−2534.
(37) Schäferling, M.; Yin, X.; Engheta, N.; Giessen, H. Helical Plasmonic Nanostructures as Prototypical Chiral Near-Field Sources. *ACS Photonics* **2014**, *1*, 530−537.
(38) Gansel, J. K.; Thiel, M.; Rill, M. S.; Decker, M.; Bade, K.; Saile, V.; von Freymann, G.; Linden, S.; Wegener, M. Gold helix photonic metamaterial as broadband circular polarizer. *Science* **2009**, *325*, 1513−1515.
(39) Gibbs, J. G.; Mark, A. G.; Eslami, S.; Fischer, P. Plasmonic nanohelix metamaterials with tailorable giant circular dichroism. *Appl. Phys. Lett.* **2013**, *103*, 213101.
(40) Gibbs, J. G.; Mark, A. G.; Lee, T.-C.; Eslami, S.; Schamel, D.; Fischer, P. Nanohelices by shadow growth. *Nanoscale* **2014**, *6*, 9457−9466.
(41) Höflich, K.; Yang, R. B.; Berger, A.; Leuchs, G.; Christiansen, S. The direct writing of plasmonic gold nanostructures by electron-beam-induced deposition. *Adv. Mater.* **2011**, *23*, 2657−2661.
(42) Esposito, M.; Tasco, V.; Todisco, F.; Benedetti, A.; Sanvitto, D.; Passaseo, A. Three Dimensional Chiral Metamaterial Nanospirals in the Visible Range by Vertically Compensated Focused Ion Beam Induced Deposition. *Adv. Opt. Mater.* **2014**, *2*, 154−161.
(43) Esposito, M.; Tasco, V.; Cuscunà, M.; Todisco, F.; Benedetti, A.; Tarantini, I.; Giorgi, M. D.; Sanvitto, D.; Passaseo, A. Nanoscale 3D Chiral Plasmonic Helices with Circular Dichroism at Visible Frequencies. *ACS Photonics* **2015**, *2*, 105−114.
(44) Hung, J.; Gao, W.; Tam, W. Y. Optical activities of micro-spiral photonic crystals fabricated by multi-beam holographic lithography. *J. Opt.* **2011**, *13*, 095102.
(45) Kuzyk, A.; Schreiber, R.; Fan, Z.; Pardatscher, G.; Roller, E.-M.; Högele, A.; Simmel, F. C.; Govorov, A. O.; Liedl, T. DNA-based self-assembly of chiral plasmonic nanostructures with tailored optical response. *Nature* **2012**, *483*, 311−314.
(46) Shen, X.; Song, C.; Wang, J.; Shi, D.; Wang, Z.; Liu, N.; Ding, B. Rolling up gold nanoparticle-dressed DNA origami into three-dimensional plasmonic chiral nanostructures. *J. Am. Chem. Soc.* **2012**, *134*, 146−149.
(47) Zhang, L.; Deckhardt, E.; Weber, A.; Schönenberger, C.; Grützmacher, D. Controllable fabrication of SiGe/Si and SiGe/Si/Cr helical nanobelts. *Nanotechnology* **2005**, *16*, 655−663.
(48) Esposito, M.; Tasco, V.; Todisco, F.; Cuscunà, M.; Benedetti, A.; Sanvitto, D.; Passaseo, A. Triple-helical nanowires by tomographic rotatory growth for chiral photonics. *Nat. Commun.* **2015**, *6*, 6484.
(49) Kaschke, J.; Wegener, M. Gold triple-helix mid-infrared metamaterial by STED-inspired laser lithography. *Opt. Lett.* **2015**, *40*, 3986−3989.
(50) Rossouw, D.; Botton, G. A. Resonant optical excitations in complementary plasmonic nanostructures. *Opt. Express* **2012**, *20*, 6968−6973.
(51) Hendry, E.; Mikhaylovskiy, R. V.; Barron, L. D.; Kadodwala, M.; Davis, T. J. Chiral electromagnetic fields generated by arrays of nanoslits. *Nano Lett.* **2012**, *12*, 3640−3644.
(52) Weiss, T.; Granet, G.; Gippius, N. A.; Tikhodeev, S. G.; Giessen, H. Matched coordinates and adaptive spatial resolution in the Fourier modal method. *Opt. Express* **2009**, *17*, 8051−8061.
(53) Lindell, I. V.; Sihvola, A. H.; Tretyakov, S.; Viitanen, A. J. *Electromagnetic Waves in Chiral and Bi-Isotropic Media*; Artech House: London, 1994.
(54) There is some special method called "diffuse reflectance circular dichroism", which probes the chirality of surfaces. However, it uses diffuse reflection and not the specular reflection as in the method we propose.[63]
(55) Sihvola, A. H.; Lindell, I. V. Bi-isotropic constitutive relations. *Microw. Opt. Technol. Lett.* **1991**, *4*, 295−297.
(56) Svirko, Y. P.; Zheludev, N. I. *Polarization of Light in Nonlinear Optics*; Wiley-VCH: New York, 1998.
(57) Yin, X.; Schäferling, M.; Metzger, B.; Giessen, H. Interpreting chiral nanophotonic spectra: the plasmonic born-kuhn model. *Nano Lett.* **2013**, *13*, 6238−6243.
(58) Nafie, L. A. *Vibrational Optical Activity: Principles and Applications*; Wiley-VCH: New York, 2011.

DOI: 10.1021/acsphotonics.6b00147
ACS Photonics 2016, 3, 1076−1084

(59) Sanz, J. M.; Ortiz, D.; Alcaraz de la Osa, R.; Saiz, J. M.; González, F.; Brown, A. S.; Losurdo, M.; Everitt, H. O.; Moreno, F. UV Plasmonic Behavior of Various Metal Nanoparticles in the Near- and Far-Field Regimes: Geometry and Substrate Effects. *J. Phys. Chem. C* **2013**, *117*, 19606−19615.
(60) Liu, N.; Guo, H.; Fu, L.; Kaiser, S.; Schweizer, H.; Giessen, H. Three-dimensional photonic metamaterials at optical frequencies. *Nat. Mater.* **2008**, *7*, 31−37.
(61) Onishi, M.; Crabtree, K.; Chipman, R. A. Formulation of rigorous coupled-wave theory for gratings in bianisotropic media. *J. Opt. Soc. Am. A* **2011**, *28*, 1747−1758.
(62) Li, L. Use of Fourier series in the analysis of discontinuous periodic structures. *J. Opt. Soc. Am. A* **1996**, *13*, 1870−1876.
(63) Bilotti, I.; Biscarini, P.; Castiglioni, E.; Ferranti, F.; Kuroda, R. Reflectance circular dichroism of solid-state chiral coordination compounds. *Chirality* **2002**, *14*, 750−756.

DOI: 10.1021/acsphotonics.6b00147
ACS Photonics 2016, 3, 1076−1084